AI-driven modeling and prediction of mechanical properties of additively manufactured Al-6061/B₄C composite

D. Kumar [1] ⓘ**, S. Singh** [2]**, P.K. Karsh** [3] ⓘ**, A. Chauhan** [4] ⓘ**, G. Saini** [4] ⓘ**, A. Chouksey** [5] ⓘ**,**

P. Kumar [1]ⓘ✉

[1] Maharishi Markandeshwar (Deemed to be University), Mullana, Ambala, India

[2] Chandigarh Engineering College, Punjab, India

[3] Parul Institute of Engineering and Technology, Parul University, Vadodara, India

[4] Panjab University SSG Regional Centre Hoshiarpur, Punjab, India

[5] Deenbandhu Chhotu Ram University of Science and Technology, Haryana, India

✉ kumar.d041789@gmail.com

ABSTRACT
This study investigates the effects of friction stir processing on the mechanical and damping properties of Al-6061 aluminum alloy, reinforced with boron carbide (B₄C) nanoparticles. A CNC milling machine was used to conduct friction stir processing, varying key processing parameters such as rotational speed, feed rate, and the number of passes. The mechanical properties analyzed include ultimate tensile strength, yield strength, natural frequency, and damping ratio. An advanced machine learning approach was implemented using a long short-term memory model optimized with the sine cosine algorithm to predict the processed material's attributes. The experimental findings demonstrate that friction stir processing significantly enhances damping characteristics due to grain refinement, with the highest damping efficiency observed at 1400 rpm. Higher rotational speeds resulted in a notable increase in yield strength, attributed to finer grain structures. The introduction of B₄C nanoparticles further improved damping properties. Additionally, the study found that an increased number of friction stir processing passes decreased shear modulus and natural frequency while increasing the loss factor and damping ratio. The developed machine learning model achieved high predictive accuracy, with R^2 values of 0.981 for the ultimate tensile strength, 0.991 for YS, 0.973 for natural frequency, and 0.995 for damping ratio. The special relativity search-optimized long short-term memory model outperformed other approaches, attaining R^2 values ranging from 0.961 to 0.998 during training and 0.919 to 0.992 during testing. These findings highlight the effectiveness of friction stir processing in enhancing material properties and the superior predictive capability of machine learning models in capturing the effects of processing parameters.

KEYWORDS
FSP • CNC • Al-6061 • microstructural evolution • material toughness • deformation desistance • LSTME optimization techniques • SRS

Introduction

Friction stir processing (FSP) is a material processing technology that operates without melting and is based on the principles of friction stir welding (FSW) [1]. It is utilized to modify the microstructure and properties of materials, specifically metals and alloys. In the FSP procedure, a specially designed rotating tool is introduced into the material

and maneuverer along the designated trajectory [2]. The rotating tool generates heat via friction, resulting in the material softening without beyond its melting point. As the instrument advances, it mechanically stirs the substance, resulting in the disintegration and redistribution of the microstructure [3]. Upon completion of the stirring process, the material is allowed to cool and undergo recrystallization, resulting in a more refined microstructure with improved mechanical properties. Friction stir processing (FSP) is a commonly employed method for objectives including grain structure refinement, alloy component homogenization, microstructural modification, surface enhancement, and defect rectification in castings and welds [4]. The method is versatile and can be used to a wide range of metallic materials, including aluminum, magnesium, titanium, steel, and their alloys. FSP offers numerous advantages over traditional processing techniques, including reduced operating temperatures, minimized distortion, and improved mechanical properties [5].

Friction stir processing (FSP) significantly improves specific mechanical properties of materials [6]. FSP does this by enhancing the microstructure of materials, resulting in a more uniform grain distribution and a reduction in grain size [7]. This refinement frequently enhances the material's tensile strength, becoming it more resilient and less susceptible to deformation. Similar to tensile strength, FSP improves the yield strength of materials by refining the grain structure and promoting a more uniform distribution of alloying elements [8]. As a result, the material demonstrates enhanced resistance to deformation and can endure greater levels of stress prior to yielding. FSP can alter the microstructure and texture of materials, hence affecting their intrinsic frequency. Friction stir processing (FSP) enhances the natural frequency of materials by refining the grain structure and introducing compressive residual stresses, hence increasing their applicability for applications requiring high vibration resistance [9]. FSP may improve the damping characteristics of materials by generating fine, equiaxed grains and promoting a more uniform distribution of alloying elements. Microstructural refinement enhances the material's ability to absorb mechanical energy, resulting in an increased damping ratio and improved vibration-damping properties [10]. Friction stir processing (FSP) offers a versatile and cost-effective approach to improving the mechanical properties of materials, rendering it applicable across several sectors. The capacity to manufacture lightweight, robust components with enhanced durability and performance makes it an attractive option for industries that emphasize material properties [11]. The improvements make FSP-processed materials highly desirable for various applications, including aerospace, automotive, marine, and structural engineering [12]. Traditional mathematical modeling techniques and machine learning (ML) present both advantages and limitations in accurately simulating friction stir processing (FSP) [13]. The finite element method (FEM) is commonly utilized for simulating FSP. The procedure involves dividing the substance into small components and employing mathematical formulas to analyze each component [14]. The finite element method (FEM) can deliver accurate estimates regarding temperature distribution, material flow, and residual stresses during friction stir processing (FSP) [15]. Nonetheless, the finite element method (FEM) requires simplifications and assumptions, potentially leading to an inadequate depiction of the complex physical processes occurring during the finite element analysis. Analytical models, such as heat conduction and flow models, provide more straightforward

mathematical representations of FSP [16]. These models exhibit remarkable efficiency regarding computational resources and can swiftly provide estimations of essential process parameters. Nonetheless, analytical models may simplify the physics of FSP and may not adequately capture all the complexities of the process. Machine learning (ML) techniques extract complex patterns and relationships from data and can be trained to predict several aspects of FSP, including temperature distribution, material flow, and microstructure evolution. This technique can successfully capture non-linear correlations and complex interactions among process components, perhaps resulting in greater accuracy than traditional models. Nonetheless, these models require significant amounts of data for training and may overfit the training data if not sufficiently regularized [17]. Machine learning methods can achieve more accuracy than conventional mathematical modeling techniques, especially when addressing complex, non-linear interactions. Machine learning techniques typically require a significant amount of data for training, while conventional modeling approaches tend to prioritize theoretical equations and assumptions [18]. Traditional modeling methodologies are frequently more intelligible because of their dependence on physical equations and principles [19]. Conversely, machine learning models are often perceived as opaque, creating difficulties in comprehending the underlying relationships. Machine learning optimization can significantly reduce processing costs relative to traditional optimization techniques [20]. Machine learning models can learn from current data and effectively ascertain optimal parameter values, hence obviating the necessity for expensive simulations or experiments. Upon completion of training, machine learning models may be seamlessly transferred to new datasets or FSP applications with minimal further work [21]. This facilitates the effective fine-tuning of FSP parameters for diverse materials, geometries, or processing conditions. Machine learning algorithms can autonomously identify and ascertain significant attributes and correlations within the data, hence reducing the necessity for manual feature engineering. This is particularly beneficial for FSP, as the relationships between process parameters and output variables can be complex and difficult to delineate using traditional methods [22].

     This work employed aluminium alloy 6061 (Al-6061) as the matrix material in metal matrix composites (MMCs), with boron carbide (B₄C) acting as the reinforcement. Al-6061/boron carbide MMCs exhibit a combination of lightweight, remarkable strength, and wear resistance, making them suitable for various applications across multiple industries [23]. The Al-6061/boron carbide metal matrix composites possess the capability to improve mechanical properties such as strength, stiffness, wear resistance, and corrosion resistance [24]. The characteristics of boron carbide reinforcement particles can be tailored according to their volume percent and dimensions, leading to a lower density in comparison to steel [25]. This renders them ideal for lightweight applications. Advanced machine learning techniques provide a novel approach for forecasting optimal processing parameters in friction stir processing (FSP) of Al-6061 alloy augmented with boron carbide nanoparticles [26]. Our objective is to employ machine learning to efficiently optimize the FSP parameters to enhance the mechanical properties and performance of the composite material [27]. This innovative method offers a data-driven strategy to enhance the efficiency and effectiveness of the FSP process, yielding superior Al-6061/boron carbide nanocomposites tailored for high-performance applications [28].

The mechanical properties and dynamic features of the materials were evaluated under different processing circumstances. The research employed cutting-edge machine learning methods to predict the sample's attributes. This approach enhances a comprehensive model of a long short-term memory (LSTME) with the application of a sine cosine algorithm (SRS) technique. The created model was assessed in a performance evaluation with three other machine-learning methods.

Materials and Method

Matrix and Reinforcement

A sheet of aluminum alloy consisting of Al-6061 and having a thickness of 4 mm served as the foundation of the construction. For the purpose of reinforcing, the B_4C nanoparticle was utilized. The results of the chemical analysis that was carried out on the FSP tool and the aluminum alloy with the use of a spectroscopic analyzer are shown in Table 1.

Table 1. Composition of Al-6061 alloy

Elements	Si	Mg	Cu	Fe	Mn	Cr	Al
Wt. %	0.510	0.797	0.219	0.257	0.043	0.157	98.000

According to the results of the transmission electron microscopy (TEM) study, the reinforcing particles displayed a distinguished degree of purity, with a measurement of 99.9 %. Furthermore, the average size of these particles was determined to be 16 ± 5.6 nm, as seen in Fig. 1.
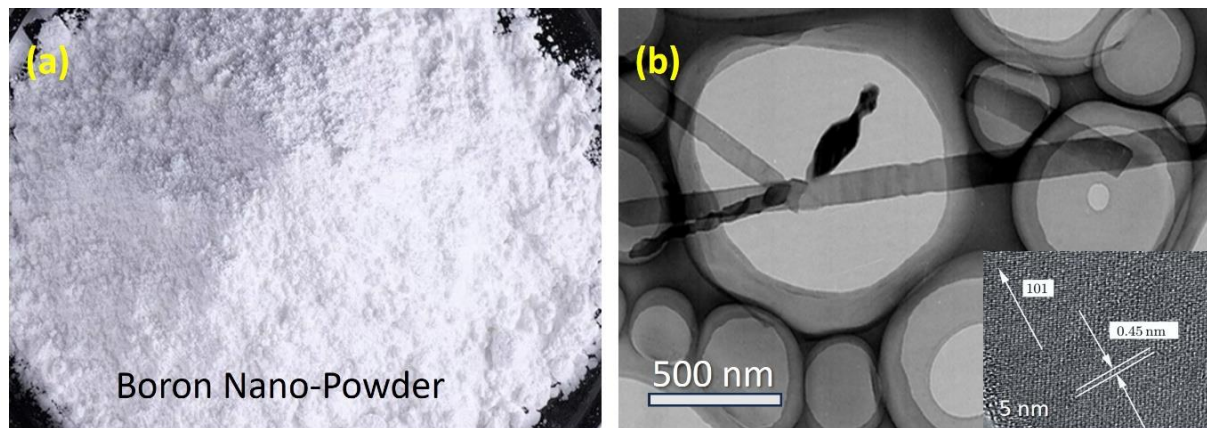
Fig. 1. (a) B_4C powder in typical form and (b) TEM Analysis of B_4C nanoparticles

Processing method

In order to change the microstructure and characteristics of a material, a solid-state joining technique known as friction stir processing (FSP) is utilized. This process makes use of frictional heat and mechanical deformation [29]. In order to form longitudinal grooves in which reinforcing particles will be included, an aluminum sheet is given the preparation necessary for milling. During the FSP process, a tool that has a taper square shape is chosen. With the tool that was chosen, the CNC milling machine is prepared for use. It is then that the tool comes into touch with the aluminum sheet that has been

prepared. As it moves down the sheet, the tool creates grooves that run in a longitudinal direction. The tool rotates at a variety of rates during this operation, including 900, 1150, 1400, and 1650 revolutions per minute, and it travels at a variety of traverse speeds, including 10, 15, and 20 mm/min throughout the procedure [30].

Fig. 2. (a) FSP processing and (b) tool dimensioning

After the FSP technique has been completed, the samples are subjected to grinding using silicon carbide paper that has grit sizes ranging from 220 to 2500. This is done in order to remove any surface flaws that may now exist. A water wash is subsequently performed on the ground samples in order to remove any abrasive residue or metal particles that may have been present. We use a solution that consists of three milliliters of hydrofluoric acid with a concentration of fifty percent, eight milliliters of a solution of nitric acid, and seventy milliliters of filtered water as the solvent. This solution is used to etch the samples. For the purpose of revealing both the microstructure and the macrostructure of the materials that have been treated, this etching method is carried out at room temperature. Until the required degree of surface quality is attained, the etched samples are examined in great detail in order to investigate the microstructure and macrostructure of the materials that have been treated. Etching is used to clean samples before they are then subjected to analysis.

In order to determine the magnitude of the treated region, we extracted dog bone-shaped samples from the central portion of the treated zone and sliced them into flat pieces. According to the criteria established by ASTM, these samples were sliced. To carry out the tensile testing, a universal testing machine (UTM) with a maximum load capacity of one hundred kilonewtons was deployed. Specific dimensions were required for the samples in accordance with the standards of ASTM B557: The width is 13 mm, the thickness of the sheet is 6 mm, the gauge length is 50 mm, the parallel length is 100 mm, the grab section length is 70 mm, and the shoulder radius is 5 mm. Through an examination of the composite surface's free vibration, the scientists were also able to determine the natural frequency and damping factor of the surface materials. The authors decided to connect accelerometers to the cut samples and monitor the vibration response of the material in order to gain a better understanding of how the material deteriorates over time.
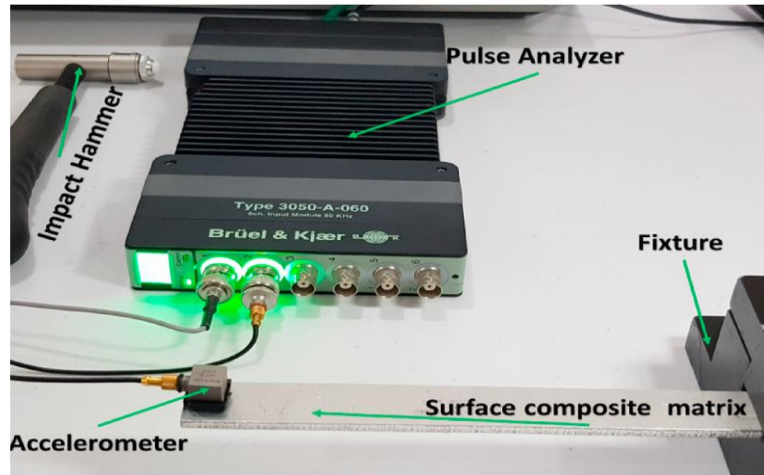
Fig. 3. 3050 Pulse analyzer to evaluate free impact vibration

A pulse data analyzer (3050 K&B vibration analyzer, Denmark) and an impact hammer (8206 K&B vibration analyzer, Denmark) were utilized in order to accomplish this task. The free vibration experiment was carried out five times as part of the procedure to guarantee the accuracy of the findings. The frequency response function (FRF), damping ratio, and fundamental frequencies of the material were all estimated via a modal analysis application known as I Scope.

Special Relativity Search Modeling Approach

One of the innovative approaches to modeling is known as the special relativity search (SRS) technique. SRS provides a fresh viewpoint on the optimization of machine learning models, and it is influenced by ideas from theoretical physics, in particular special relativity.
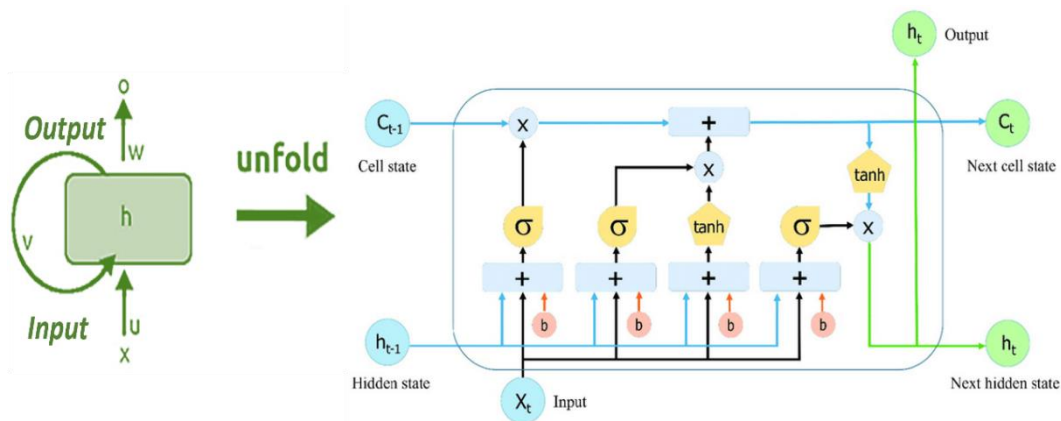

Fig. 4. Systematic view of LSTME network

The concept of relativistic transformations is the fundamental idea behind SRS. In this kind of transformation, variables are dynamically altered according to the relative significance they hold and the contribution they make to the overall performance of the model. SRS takes into consideration the inherent linkages and dependencies among variables, which is analogous to the relativistic effects that are observed in high-speed

motion. This is in contrast to typical optimization approaches, which handle variables in a uniform manner. The following are important elements that make up the SRS.

The variable transformation: variables undergo a transformation that is comparable to the relativistic effects, in which their values are modified according to the relevance of the variables in relation to other variables and the overall purpose of the model.
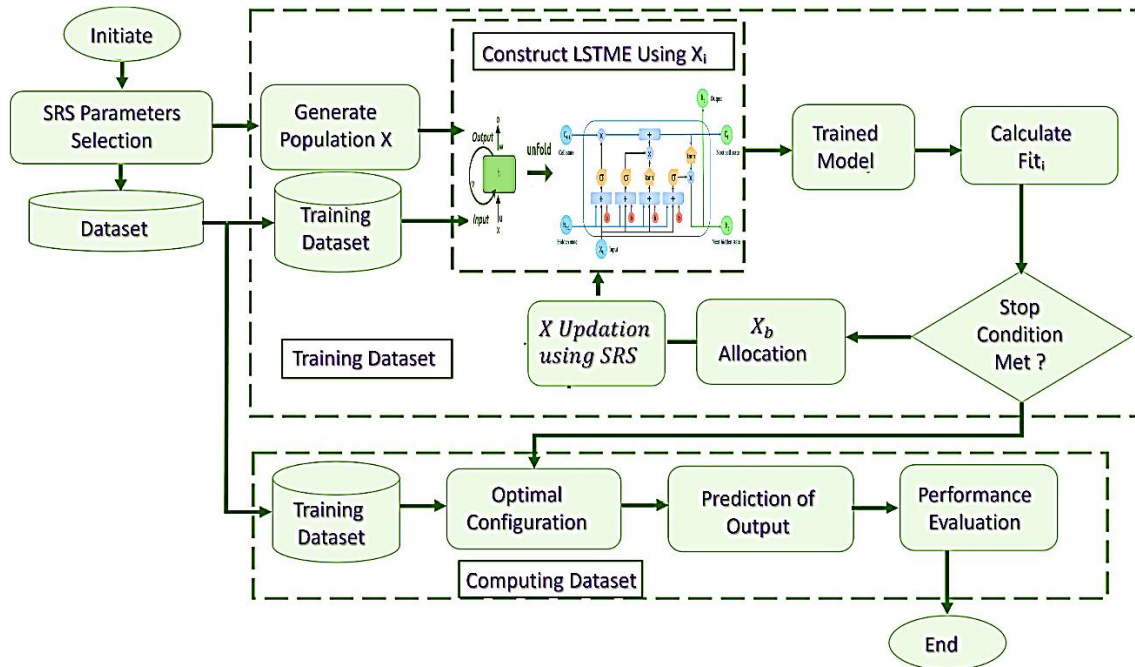

Fig. 5. Special relativity search-based LSTME network model

The concept of dynamic scaling is analogous to the concept of time dilation in special relativity. It is possible for variables to undergo dynamic scaling dependent on the relative significance of the variables. To guarantee that the model remains balanced while giving essential variables a larger weightage, this ensures that the model meets the requirements.

Velocity-based optimization: special relativistic systems (SRS) use velocity-based optimization approaches to iteratively tune variable transformations. These techniques are inspired by the idea of velocity in special relativity. The model is able to dynamically adapt to changing data dynamics and optimization goals as a result of this.

Not only does SRS take into account the spatial correlations between variables, but it also takes into account the temporal dynamics of those variables. Because of this, the model is able to recognize complex patterns and relationships across time, which greatly improves its ability to make accurate predictions.

Nonlinear transformations: SRS makes use of nonlinear transformations in order to capture both complicated relationships and interactions among variables. This helps to improve the expressiveness of the model as well as its ability to accurately predict future outcomes.

Results and Discussions

Dynamic characteristics

The results of the research investigation, which are presented in Figs. 6−8, unequivocally demonstrate that there is a direct connection between the FSP Parameters and the damping ratio. However, the capacity to reduce vibrations may be enhanced at a specific ideal rotational velocity. This is something that can be done.
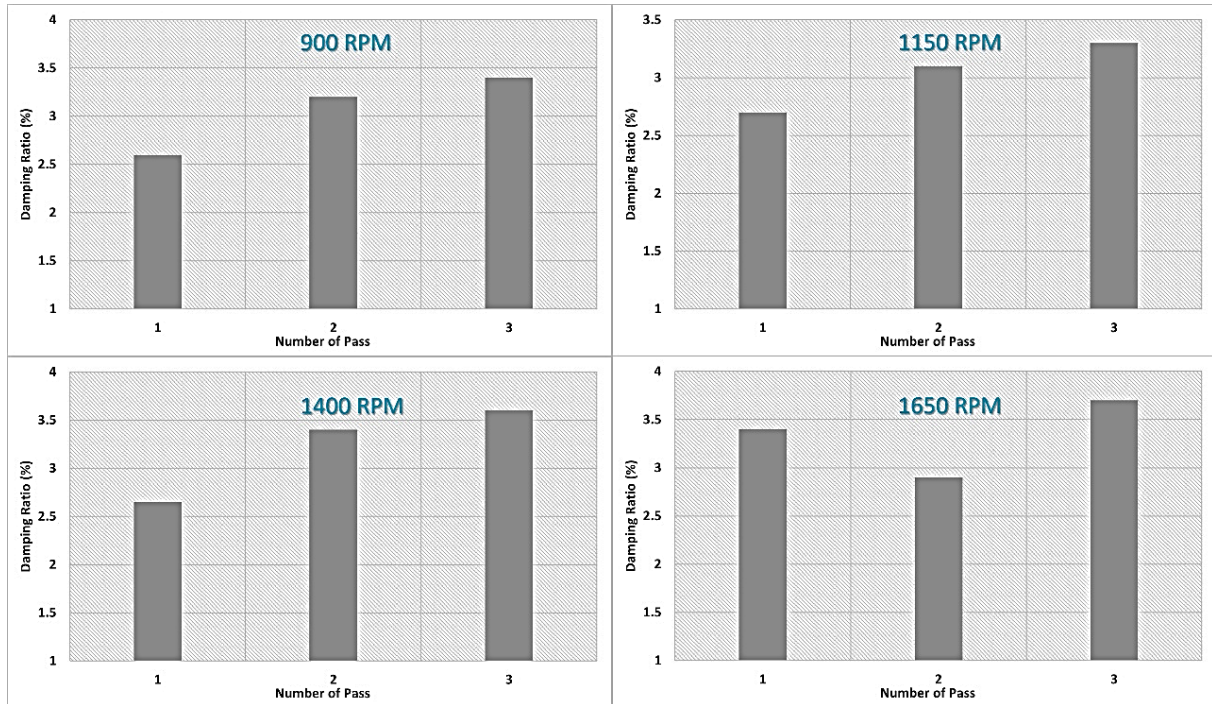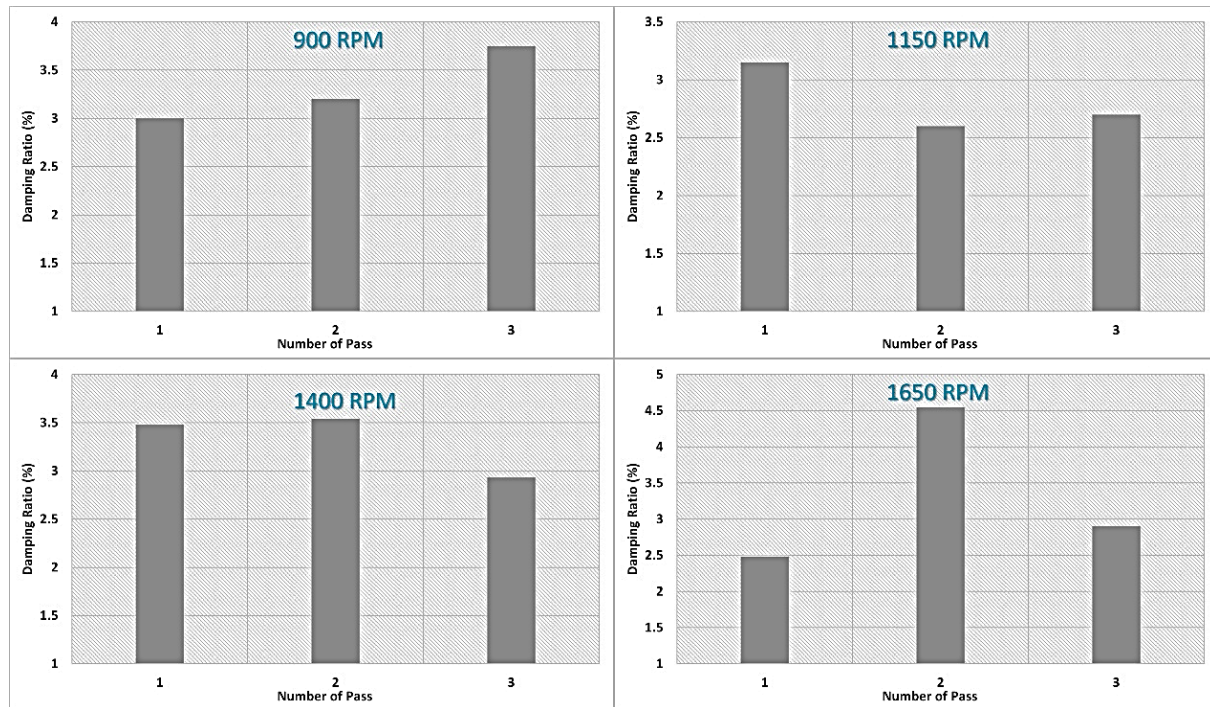

Fig. 6. Damping capacity of the samples at a traverse speed of 10 mm/min
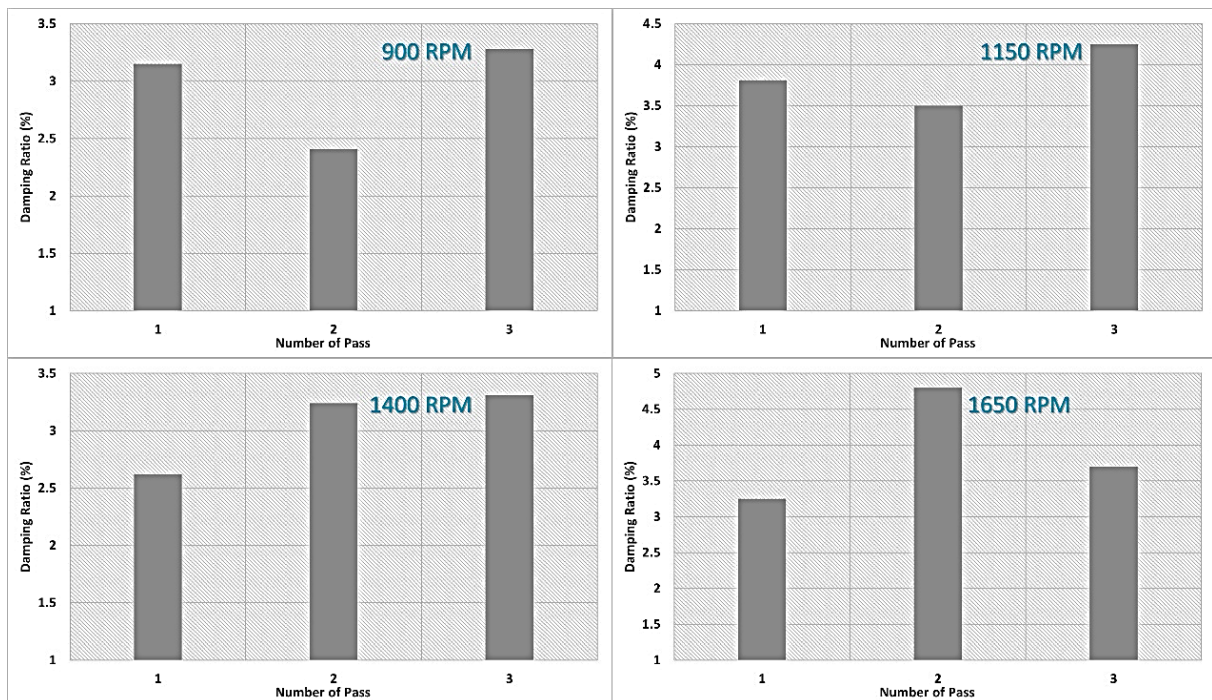
Fig. 7. Sample's damping ratio at 15 mm/min traverse speed

Fig. 8. Damping capacity of the samples at a traverse speed of 20 mm/min

According to the technical point of view, the rotational speed was set at 900 revolutions per minute, which resulted in the highest degree of damping capabilities being attained in all of the testing scenarios. One may have a better understanding of the events by examining the link that exists between the rate of thermal energy creation and the rotational velocity. The microstructure becomes more uniform and finely distributed as a result of the breakdown of the constituent grains of the material, which is induced by the excessive heat. There is an improvement in its capacity to absorb and reduce vibrations as a result of the increased density of its streamlined shape.

Based on the statistical study, it was determined that the damping capacity did not change regardless of the pace of travel. Specifically, this can be related with two primary variables: There is a possibility that the experiment's travel speed range was too limited to find any obvious change in damping capacity. This is something that may be considered at first appearance.

There is a possibility that the oscillations in damping capacity numbers are responsible for concealing the actual impact of transit speed. By incorporating boron carbide nanoparticles into the metal matrix, the vibration dampening capabilities of the material were significantly improved. In order to achieve this improvement, it was established that the concentration of nanoparticles in the matrix was the most important parameter. As the ratio of nanoparticles was raised, there was a corresponding rise in the improvement of damping capacity that was observed.

When the number of passes is increased, the natural frequency of the samples decreases in proportion to the increase. Repetitive agitation of the instrument results in the breakdown of material particles, which in turn leads to a reduction in stiffness and the subsequent production of this phenomena. However, increasing the number of passes results in samples that have a higher damping ratio. This is the opposite of what you

would expect. As a result of the agitating action, the grain structure is improved, which in turn increases the presence of flaws and improves the grain's ability to collect and absorb vibrations. In a similar vein, the sample loss factor will increase in proportion to the growing number of different passes. Because of the presence of a grain structure that is more accurate, there has been an increase in the amount of frictional losses recorded. During vibration, the amount of energy that is transformed into heat is quantified by the loss factor, which is the opposite of the energy conversion factor. Increasing the number of passes also results in a decrease in the retained modulus of the samples. There is a high probability that the reason is the deterioration of the grain structure, which leads to a decreasing elasticity. Increasing the number of passes results in a loss modulus trend that is comparable to the one we saw in the samples. The main justification for this occurrence is supplied by the loss modulus, which quantifies the energy dissipation that happens during vibration; materials with finer grain patterns show higher levels of frictional losses. This is the core rationale for this occurrence.

Table 2. Significant Process Parameters of FSP Process

| Rotational speed, rpm	Number of passes	Transverse speed, mm/min	Damping ratio (ζ)	Loss factor	Shear modulus, MPa
1650	3	20	2.98	0.058	26.12
900	3	15	3.57	0.072	25.91

The differences in the dynamic properties of the samples at different RPMs are summarized in Table 2, which gives a short summary of the subject matter. The natural frequency of each specimen decreases as the revolutions per minute (RPM) rises. This occurs as a result of the increased heat generated by the greater spinning speed, which leads to the grain structure being more disorganized and the material becoming less rigid. In spite of the fact that the samples indicate a decrease in stiffness, the damping ratio demonstrates an increase as the RPMs climb. The reason for this is because the grain structure has been polished much further, which makes it possible for imperfections to absorb and attenuate vibrations more effectively. Increasing the rotational speed also results in a rise in the loss factor, which is a measurement of the amount of energy that is lost during vibration. At faster speeds, the grain structure becomes finer, which results in larger frictional losses. This is the reason why this is the case. The shear modulus of the samples falls as the revolutions per minute (RPM) increases. The frequent agitation of the tool is responsible for this phenomenon. This agitation causes the particles of the material to break down, which ultimately leads to a reduction in the material's flexibility. The loss modulus of the sample, which is a measure of the amount of energy that is lost during vibration, likewise increases as the speed at which the sample is spinning increases. When rotational velocities are raised, a finer grain structure is formed, which results in increased frictional losses. This is the reason why this circumstance occurs. A direct association exists between the rise in the complex moduli of the samples and the increase in rotational speed. This correlation also exists between the two variables. The complex modulus is a mathematical representation of the overall stiffness and damping qualities of the material. Shear modulus of the samples decreases as the revolutions per minute (RPM) increases. The rationale for this is because increasing the RPMs makes it

more difficult to shear the grain structure that is smaller, which ultimately results in a reduction in the shear strength. The results of this study demonstrate that the dynamic characteristics of the samples are altered when the rotational speed of the samples increases during the processing phase.

The results of the study indicate that there is a clear connection between the rate of rotation and a number of dynamic properties of the specimens. As the revolutions per minute (RPM) increases, the natural frequency and shear modulus drop. This is because the increase in dampening ratio and loss factor was observed to be the reason for the decline. According to the findings of the study, friction stir processing has the potential to significantly improve the damping capabilities of materials by producing a grain structure composition that is more refined. This more finely structured grain structure makes it possible to inject a greater number of faults into the material, which in turn helps the material to more effectively catch and absorb vibrations. As an additional point of interest, the findings provide light on the connection that exists between the speed at which an object is moving and its capacity to dampen vibrations. The dampening effect is also enhanced by traverse speed, which is similar to the impact of rotational speed. The greater thermal energy that is created during the process assists in dissolving granules, which in turn reduces the stiffness of the encapsulated particles. Additionally, the creation of a finer grain structure at greater traversal speeds increases the presence of defects in the material, which in turn enhances the material's capacity to catch and absorb vibrations.

Mechanical properties

The grain structure is refined using the friction stir surface processing, which has a major impact on the mechanical properties of the materials through its use. A highly prominent average grain size of around 142 μm is observed in the earliest stages of the Al-6061 base alloy, which exhibits an aspect ratio of approximately 32.3 % within the initial stages. As a result of three rounds of FSP, the average grain size falls to 12.92 μm, while the aspect ratio increases to 91.8 %.
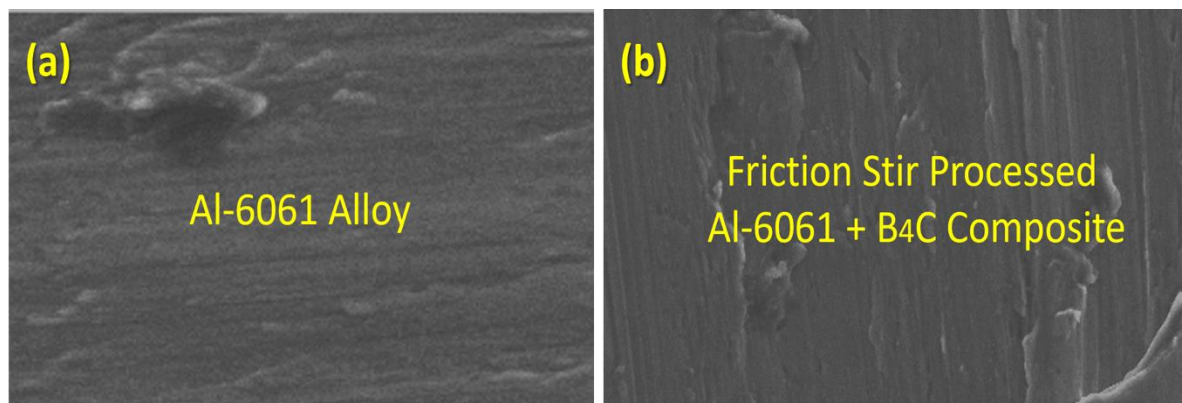

Fig. 9. Optical microscope (a) Al-6061 alloy and (b) Al-6061/B₄C FSP-ed composite

The microstructure picture shown in Fig. 9 illustrates that a reduction in grain size is a strong indicator that the grain structure has been successfully refined by FSP. The

results of the investigation suggest that there is a connection between the mechanical characteristics and the rotating speed of the instrument.
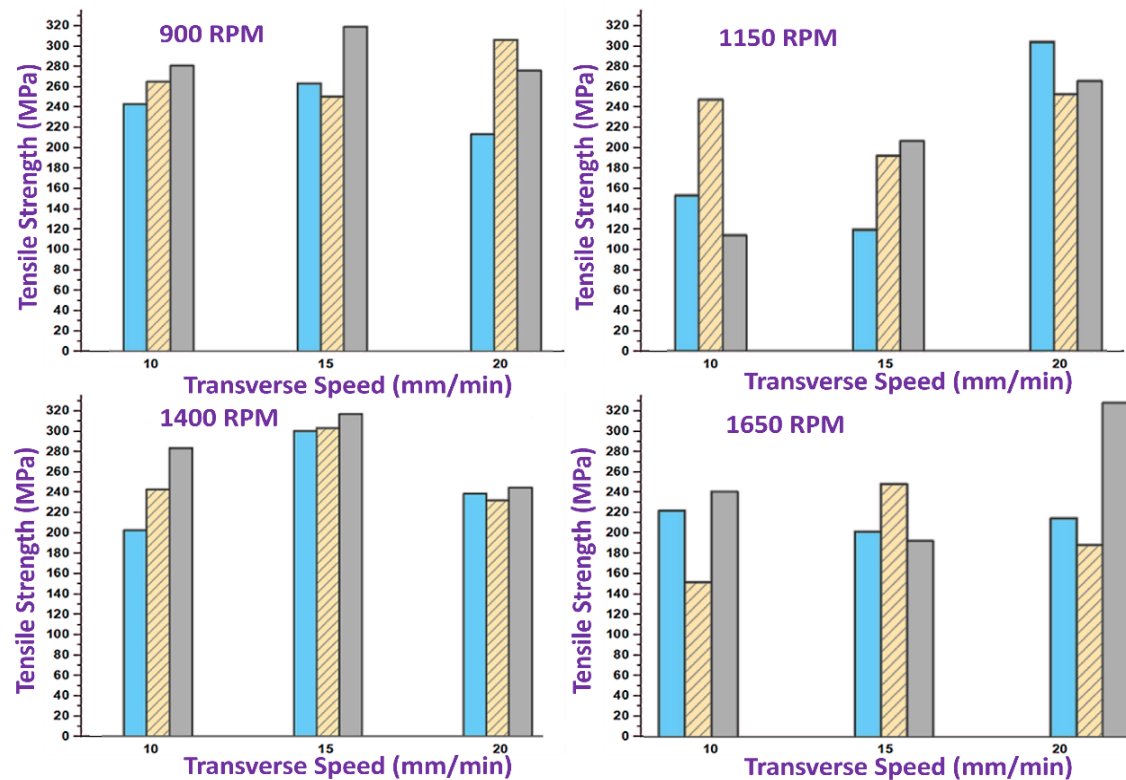
Fig. 10. Tensile strength of the specimens at different RPM (a) 900 RPM, (b) 1150 RPM, (c) 1650 RPM and (d) 1400 RPM
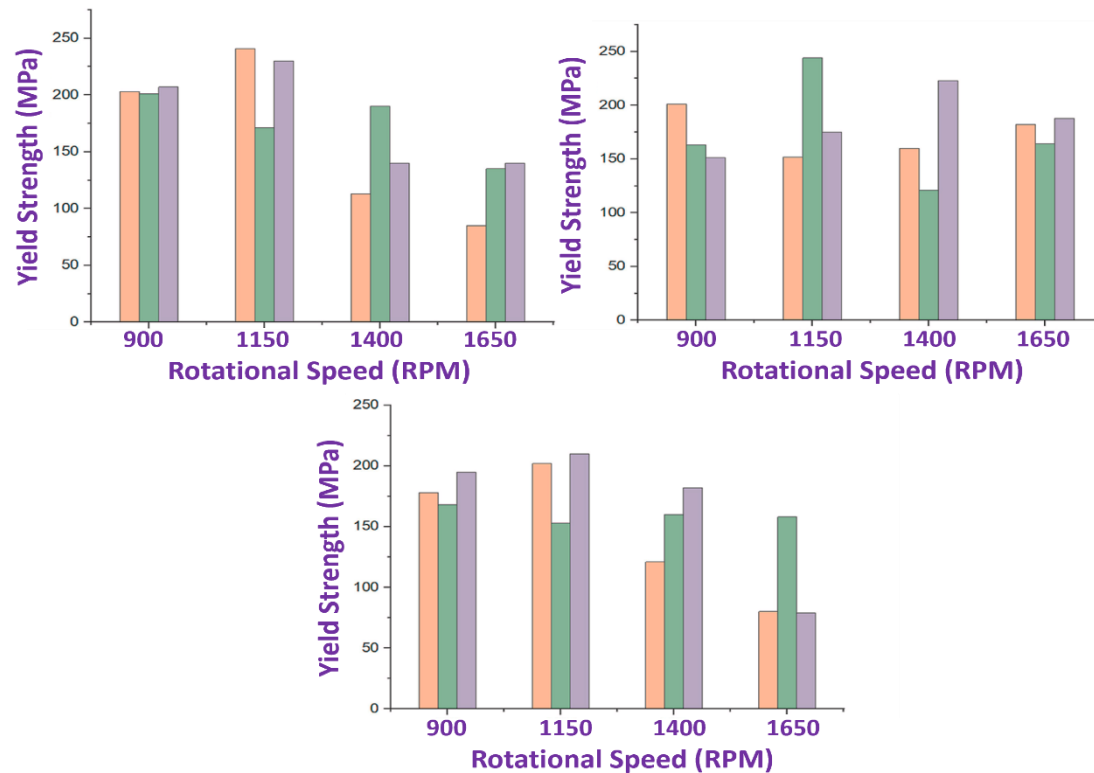
Fig. 11. Yield strength of the specimens at different RPM

It has been observed that the rotating speeds have a beneficial impact on the ultimate tensile strength (UTS) and yield strength (YS) of the samples, which ultimately results in the increase of these properties (Figs. 10 and 11). There is a clear correlation between the higher speeds, which creates more heat, and the disintegration of grains, which is a direct result of the stronger material. The more finely organized microstructure that results from higher rotational velocities is responsible for the increased yield strength of the material. Additionally, the material's capacity to tolerate deformation is enhanced, which leads to an increase in the material's yield strength. Increasing the number of FSP passes results in a drop in both the yield and ultimate tensile strengths (UTS and UTS, respectively). As a result of the frequent agitation of the instrument, the grains gradually get fragmented, which ultimately compromises the structural integrity of the material. In a similar vein, decreasing the feed rate causes a slower dissipation of heat, which in turn leads to a drop in mechanical properties as a result of less grain disintegration.

Predicted results

In order to make predictions about the characteristics of the processed data, this research endeavor makes use of four different machine-learning models. The UTS, YS, natural frequency, and damping ratio are all included in the models respectively (Fig. 12–15). In contrast to the subsequent three models, which combine LSTME with optimization strategies, the first model is an independent LSTME. The LSTME-FHO, the LSMTE-SRS, and the LSTME-DMOA are some of the optimization strategies that are discussed in this article. Both the training and testing of the models are carried out with the use of empirical data.

The remaining thirty percent of the data is reserved for testing, while seventy percent of the data is given up to training. In order to evaluate the effectiveness of each model, three different indicators of accuracy are utilized. The root mean square error (RMSE), the coefficient of determination (R^2), and the mean absolute error (MAE) are the metrics that are utilized in this study.
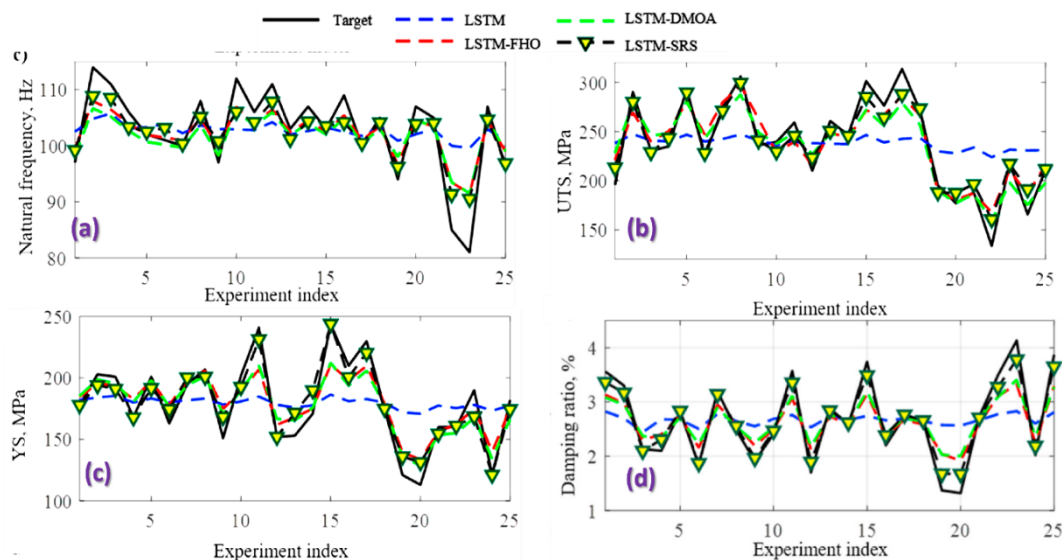

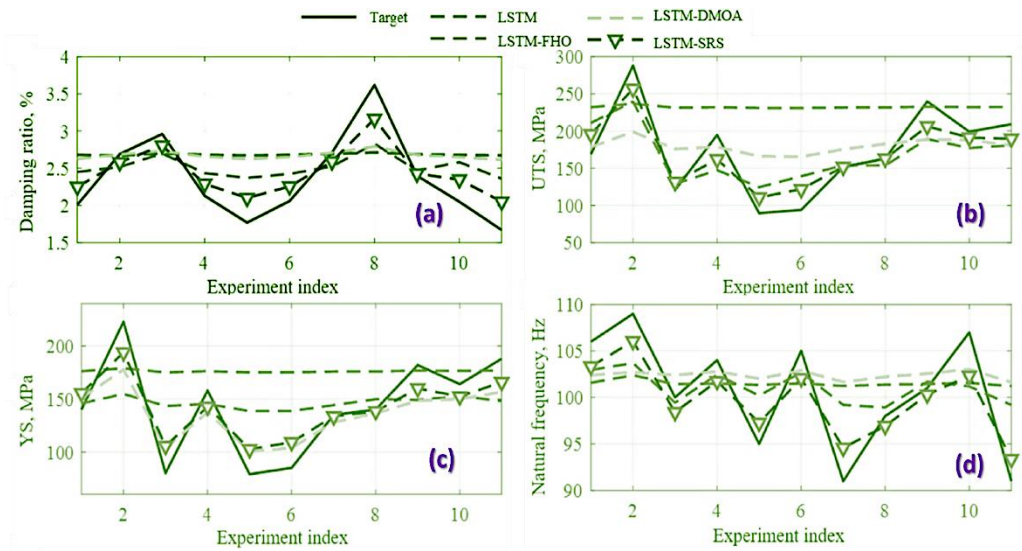**Fig. 12.** Training process of experimental and predicted data

Fig. 13. Testing process of experimental and predicted data
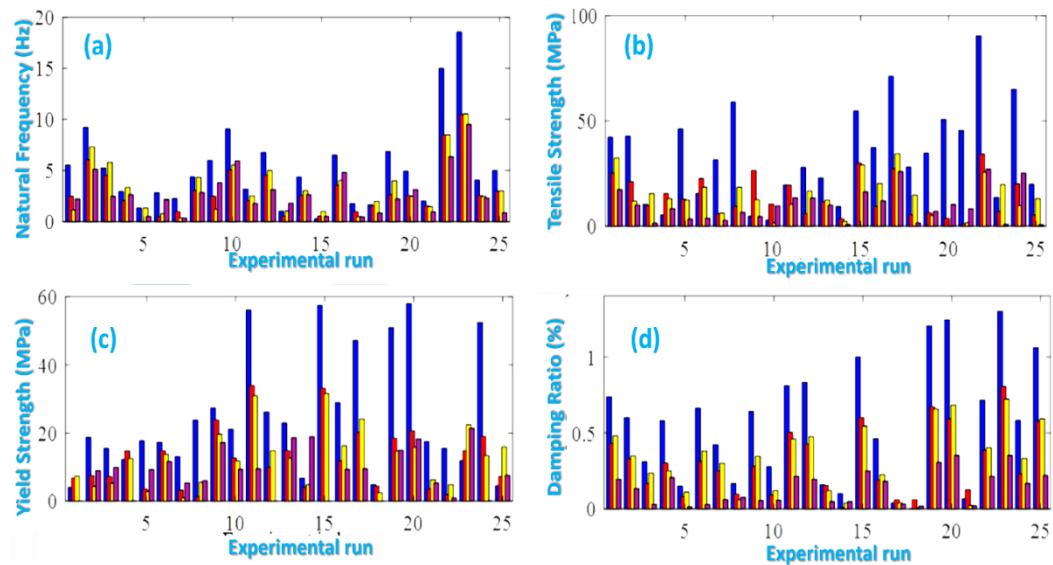

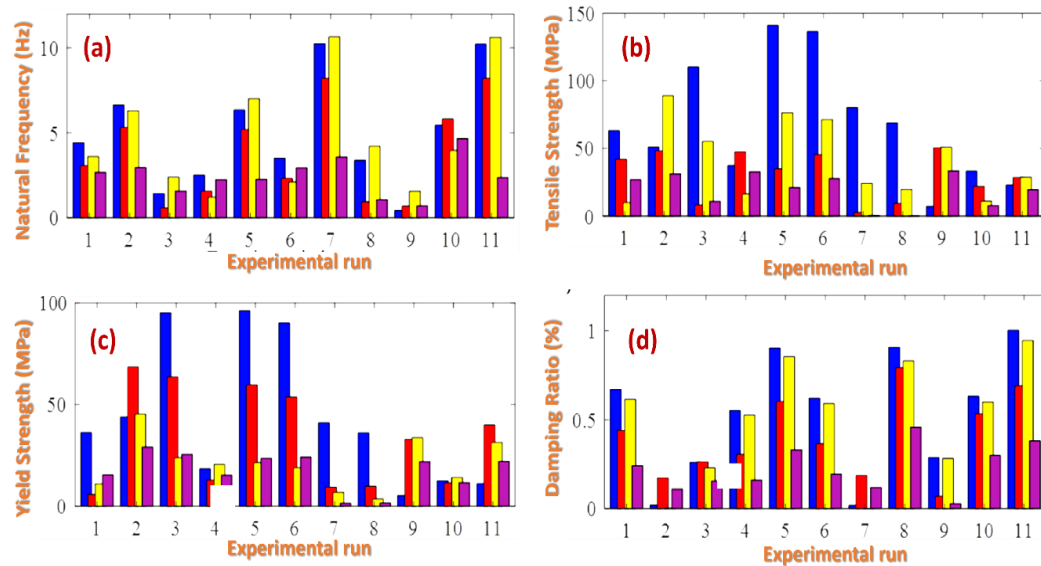**Fig. 14.** Training processing error of experimental and predicted data


Fig. 15. Testing processing error of experimental and predicted data

According to the findings, there is a significant connection between the data that was obtained through experimentation and the data that was projected. When compared to the performance of all of the other models that were used, the LSTME-SRS model demonstrated higher performance, with the LSTME-DMOA and LSTME-FHO models following closely behind a close second. Throughout the entirety of the training and testing stages, the independent LSTME model demonstrates the least level of agreement with the experimental data.

A further demonstration of the agreement is provided by the absolute error research, which demonstrates that the LSTME-SRS consistently has the lowest error across all features. This demonstrates that it has a stronger predictive potential. The absolute errors that are exhibited by LSTME-DMOA and LSTME-FHO are relatively low when compared to the errors that are created by LSTME-SRS and the solo LSTME model.
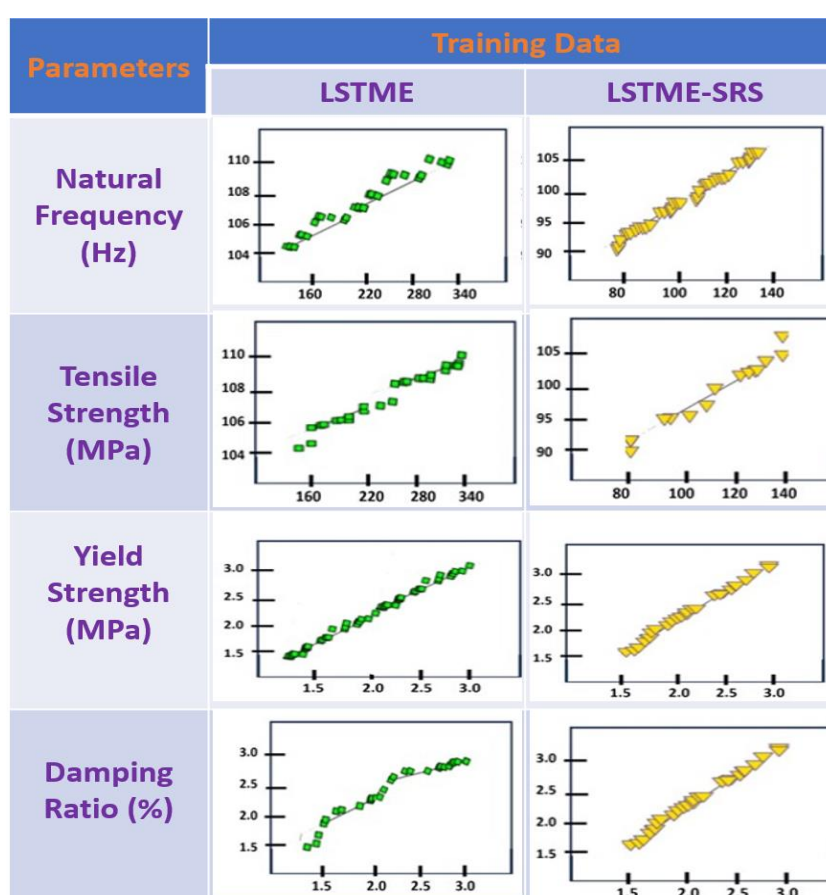
Fig. 16. QQ plots during training and testing of data

Considering the extraordinary capacity of the LSTME-SRS algorithm to generate the least amount of absolute error, it is clear that the algorithm is highly effective in accurately predicting a wide variety of characteristics of the processed data. In terms of prediction accuracy, our findings indicate that LSTME-SRS performs better than other models, which suggests that it is able to successfully anticipate the characteristics of processed data. When LSTME-DMOA and LSTME-FHO are compared to LSTME-SRS in the QQ graphs shown in Fig. 16, there is a stronger link between the anticipated data and the actual data.

The statement is made in respect to the other two ideas that have been proposed. In comparison to the other models that were examined, the single LSTME model demonstrates the least amount of connection with the available experimental data. The close connection or proximity of the yellow outcomes to the diagonal lines is evidence that the predictions produced by LSTME-SRS are accurate. This proximity can be observed in the yellow results. The projected data that was created by the independent LSTME model, which is represented by a light blue color, on the other hand, displays a higher distance from the diagonal lines. The fact that this gap exists is more evidence that LSTME-SRS performs better than LSTME, LSTME-FHO, and LSTME-DMOA in terms of performance in terms of accuracy. In order to evaluate the correctness of the models, a number of performance metrics were utilized. These metrics included R^2, MAE, and RMSE measures.

Table 3. Machine-learning model and performance measures

Properties	Models	Training data			Testing data		
		R^2	RMSE	MAE	R^2	RMSE	MAE
Ultimate tensile strength, MPa	LSTME-SRS	0.969	12.446	9.735	0.916	22.820	19.373
	LSTME-FHO	0.903	16.867	1.399	0.708	65.429	30.877
	LSTME-DMOA	0.899	17.088	14.439	0.889	49.553	41.315
	LSTME	0.792	40.970	34.291	0.725	81.095	68.701
Yield strength, MPa	LSTME-SRS	0.971	10.878	8.539	0.958	19.681	17.526
	LSTME-FHO	0.907	15.444	12.581	0.760	40.988	33.503
	LSTME-DMOA	0.948	15.137	12.636	0.939	24.136	21.052
	LSTME	0.886	30.813	25.397	0.865	55.295	44.406
Natural frequency, Hz	LSTME-SRS	0.982	2.817	2.232	0.957	2.697	2.475
	LSTME-FHO	0.969	5.785	4.478	0.714	4.715	3.824
	LSTME-DMOA	0.928	5.610	4.435	0.849	5.875	4.900
	LSTME	0.671	6.707	5.260	0.544	5.866	4.984
Damping ratio (ζ)	LSTME-SRS	0.997	0.173	0.139	0.990	0.259	0.228
	LSTME-FHO	0.993	0.376	0.309	0.827	0.461	0.407
	LSTME-DMOA	1.004	0.389	0.318	0.982	0.592	0.501
	LSTME	0.750	0.691	0.567	0.728	0.632	0.536

To make things easier for you, the findings are presented in a condensed version in Table 3. The prediction efficacy of diverse LSTM-based models for ultimate tensile strength (UTS), yield strength (YS), natural frequency, and damping ratio (ζ) is assessed utilizing statistical measures including R^2 (coefficient of determination), RMSE (root mean square error), and MAE (mean absolute error). A superior R^2 value denotes enhanced predictive accuracy, and diminished RMSE and MAE values imply decreased prediction mistakes. The LSTME-SRS model routinely surpasses others in all attributes, exhibiting exceptional predictive performance. For UTS, LSTME-SRS attains the maximum accuracy, evidenced by R^2 of 0.969 in training and 0.916 in testing, alongside the lowest RMSE (12.446 and 22.820 MPa) and MAE (9.735 and 19.373 MPa). The LSTME-FHO and LSTME-DMOA models exhibit modest accuracy, however the standard LSTME model has worse performance, achieving R^2 of just 0.725 during testing and considerably elevated error values. Likewise, for yield strength, LSTME-SRS demonstrates enhanced accuracy with R^2 of 0.971 during training and 0.958 during testing, resulting in minimum RMSE (10.878

and 19.681 MPa) and MAE (8.539 and 17.526 MPa). The foundational LSTME model is the least successful, exhibiting R^2 of 0.865 and elevated error metrics. The LSTME-SRS model yields optimal predictions for Natural Frequency, achieving R^2 of 0.982 during training and 0.957 during testing, while exhibiting minimal RMSE and MAE values. Conversely, the base LSTME model demonstrates the worst performance, achieving a testing R^2 of just 0.544. Ultimately, for the damping ratio (ζ), LSTME-SRS achieves exceptional accuracy with R^2 of 0.997 during training and 0.990 during testing, accompanied by negligible RMSE (0.173 and 0.259) and MAE (0.139 and 0.228), establishing it as the most dependable model. The LSTME-DMOA and LSTME-FHO models exhibit satisfactory performance; however, the standard LSTME model is the least successful, demonstrating R^2 of just 0.728 during testing, accompanied by considerably greater error rates. The results underscore the exceptional predictive capability of LSTME-SRS, establishing it as the most efficacious model for predicting material properties, hence providing enhanced accuracy and dependability in forecasting mechanical and vibrational characteristics.

Conclusions

The study utilized a CNC milling machine to perform FSP on Al-6061 aluminum alloy, incorporating boron carbide nanoparticles as reinforcements. The primary objective was to examine the influence of key processing parameters—feed rate, number of passes, and rotational speed—on the mechanical properties of the processed samples. Specifically, the study focused on UTS, YS, natural frequency, and damping ratio. To enhance predictive accuracy, an advanced machine learning approach was employed using LSTME model optimized with SRS. The following conclusions were mentioned follows:

1. Friction stir processing significantly improves the damping properties of Al-6061 alloy by refining the grain structure, with maximum damping efficiency observed at 1400 rpm.
2. Increasing rotational and traverse speeds enhances both mechanical properties and damping performance, while additional FSP passes improve the damping ratio but reduce the shear modulus and natural frequency.
3. The incorporation of boron carbide nanoparticles further improves damping capabilities, contributing to better material performance.
4. Higher rotational speeds generate increased thermal energy, promoting grain breakdown and finer grain structures, which enhance yield strength and overall material toughness.
5. The SRS-optimized LSTME model demonstrated high predictive accuracy, achieving R^2 values of 0.981 for UTS, 0.991 for YS, 0.973 for natural frequency, and 0.995 for damping ratio, outperforming other machine learning models.

CRediT authorship contribution statement

Dinesh Kumar 🆔Sc🅡ᴳ: writing – original draft, writing – review & editing; **Sarabjeet Singh**: writing – review & editing; **Pardeep Kumar Karsh** 🆔Sc🅡ᴳ: writing – original draft; **Abhishek Chauhan** 🆔: writing – review & editing; **Gaurav Saini** 🆔: writing – review & editing; **Arti Chouksey** 🆔Sc: writing – original draft; **Pardeep Kumar** 🆔Sc🅡ᴳ: writing – review, editing & supervision.

Conflict of interest

The authors declare that they have no conflict of interest.

References

1. Nikhil B, Govindan P. Effect of tool probe geometry on the material flow and mechanical behaviour of dissimilar AA2024 / AA7075 friction stir welded joints. *International Journal on Interactive Design and Manufacturing (IJIDeM)*. 2024;18(3): 1645–1664.

2. Paul RC, Joseph R, Nadana Kumar V, Booma Devi P, Manigandan S. Experimental analysis of hybrid metal matrix composite reinforced with Al2O3 and graphite. *International Journal of Ambient Energy*. 2022;43(1): 648–652.

3. Kumar D, Singh S, Angra S. Dry sliding wear and microstructural behavior of stir-cast Al6061-based composite reinforced with cerium oxide and graphene nanoplatelets. *Wear*. 2023;204615: 516–517.

4. Kumar D, Singh S. Enhancing friction and wear performance in hybrid aluminum composites through grey relational analysis. *Res. Eng. Struct. Mater.* 2024;10(3): 943–956.

5. Subburaj A, Antony Joseph Decruz AMM, Chandra Moorthy VA, Durairaj R. Mechanical Characterization and Micro-structural Analysis on AA2024 Hybrid Composites Reinforced with WC and Graphene Nanoparticles. *Trans Indian Inst Met*. 2022;75: 1721–1730.

6. Khiyavi BA, Aghchai AJ, Arbabtafti M, Givi MKB, Jafari J. Effect of friction stir processing on mechanical properties of surface composite of Cu reinforced with Cr particles. *Advanced Materials Research*. 2014;829: 851–856.

7. Li X, Das H, Pole M, Li L, Soulami A, Grant GJ, Herling DR, Efe M. Exceptional strength and wear resistance in an AA7075 / TiB 2 composite fabricated via friction consolidation. *Materials & Design*. 2024;242: 113006.

8. Vasu C, Durga KJAN, Srinivas I, Dariyavali S, Venkateswarlu B, Sunil BR. Developing composite of ZE41 magnesium alloy- calcium by friction stir processing for biodegradable implant applications. *Materials Today: Proceedings*. 2019;18: 270–277.

9. Molla Ramezani N, Davoodi B. Evaluating the influence of various friction stir processing strategies on surface integrity of hybrid nanocomposite Al6061. *Scientific Reports*. 2024;14: 8056.

10. Rajak DK, Pagar DD, Menezes PL, Linul E. Fiber-reinforced polymer composites: Manufacturing, properties, and applications. *Polymers*. 2019;11(10): 1667.

11. Kumar D, Angra S, Singh S. Mechanical Properties and Wear Behaviour of Stir Cast Aluminum Metal Matrix Composite: A Review. *International Journal of Engineering, Transactions A: Basics*. 2022;35(4): 794–801.

12. Kumar D, Angra S, Singh S. Synthesis and characterization of DOE-based stir-cast hybrid aluminum composite reinforced with graphene nanoplatelets and cerium oxide. *Aircraft Engineering and Aerospace Technology*. 2023;95(10): 1604–1613.

13. Kumar J, Singh D, Kalsi NS, Sharma S, Mia M, Singh J, Rahman MA, Khan AM, Rao KV. Investigation on the mechanical, tribological, morphological and machinability behavior of stir-casted Al/SiC/Mo reinforced MMCs. *Journal of Materials Research and Technology*. 2021;12: 930–946.

14. Maurya MC, Ali Jawaid SM, Chakrabarti A. Flexural Behaviour of Nanocomposite Plate with CNT Distribution and Agglomeration Effect. *Mechanics of Advanced Composite Structures*. 2023;10(1): 123–136.

15. Kumar D, Kumar P, Kumar N, Agarwal S. Microstructural, microhardness and electrical conductivity analysis of AD31T alloy processed by friction stir processing. *Multidiscipline Modeling in Materials and Structures*. 2024;20(6): 937–951.

16. Yadav A, Jain A, Verma R. Effect of rotational speed on various performance measures in friction stir lap weld of aluminium alloy 6061 using numerical simulation approach. *Materials Physics and Mechanics*. 2024;52(6): 114–125.

17. Kilimtzidis S, Kotzakolios A, Kostopoulos V. Efficient structural optimisation of composite materials aircraft wings. *Composite Structures*. 2023;303(5): 116268.

18. Hasan MS, Kordijazi A, Rohatgi PK, Nosonovsky M. Application of Triboinformatics Approach in Tribological Studies of Aluminum Alloys and Aluminum-Graphite Metal Matrix Composites. In: Srivatsan TS, Rohatgi PK, Hunyadi Murph S. (eds) *Metal-Matrix Composites. The Minerals, Metals & Materials Series*. Cham: Springer; 2022. p.41–51.

19. Agarwal S, Singh S. Production techniques and properties of particulate reinforced metal matrix composites : a review. *Materials Physics and Mechanics*. 2024;52(6): 136–153.

20. Wang Y, Wang H, Razzaghi R, Jalili M, Liebman A. Multi-objective coordinated EV charging strategy in distribution networks using an improved augmented epsilon-constrained method. *Applied Energy*. 2024;369: 123547.

21. Rao TB, Ponugoti GR. Characterization, Prediction, and Optimization of Dry Sliding Wear Behaviour of Al6061/WC Composites. *Transactions of the Indian Institute of Metals.* 2021;74(1): 159–178.

22. Jeon CH, Jeong YH, Seo JJ, Tien HN, Hong ST, Yum YJ, Hur SH, Lee KJ. Material properties of graphene/aluminum metal matrix composites fabricated by friction stir processing. *Int. J. Precis. Eng. Manuf.* 2014;15: 1235–1239.

23. Gangadharappa M, Geetha HR, Manjunath NK, Umesh GL, Shivakumar MM. Study on n-TiB2 particulates reinforced Al7075 nano composite for soil nail applications: mechanical, wear, and fracture characterizations. *Materials Physics and Mechanics.* 2024;52(6): 101–113.

24. Kumar N, Bharti A, Chauhan AK. Effect of Ti reinforcement on the wear behaviour of AZ91/Ti composites fabricated by powder metallurgy. *Materials Physics and Mechanics.* 2021;47(4): 600–607.

25. Kumar D, Singh S, Angra S. Qualitative and quantitative interdependence of physical and mechanical properties of stir-casted hybrid aluminum composites. *Materials Physics and Mechanics.* 2023;51(6): 14–23.

26. Sharath BN, Madhu KS, Pradeep DG, Madhu P, Premkumar BG, Karthik S. Effects of tertiary ceramic additives on the micro hardness and wear characteristics of Al2618 + Si3N4-B4C-Gr hybrid composites for automotive applications. *Journal of Alloys and Metallurgical Systems*. 2023;3(1): 100014.

27. Kumar D, Angra S, Singh S. High-temperature dry sliding wear behavior of hybrid aluminum composite reinforced with ceria and graphene nanoparticles. *Engineering Failure Analysis.* 2023;151(3): 107426.

28. Nirala A, Soren S, Kumar N, Kaushal DR. A comprehensive review on mechanical properties of Al-B4C stir casting fabricated composite. *Materials Today: Proceedings.* 2020;21(4): 1432–1435.

29. Raja R, Shanmugam R, Jannet S, Kumar GBV, Venkateshwaran N, Naresh K, Ramoni M. Development of Al-Mg2Si Alloy Hybrid Surface Composites by Friction Stir Processing: Mechanical, Wear, and Microstructure Evaluation. *Materials.* 2023;16(11): 4131.

30. Sharma S, Handa A, Singh SS, Verma D. Influence of tool rotation speeds on mechanical and morphological properties of friction stir processed nano hybrid composite of MWCNT-Graphene-AZ31 magnesium. *Journal of Magnesium and Alloys.* 2019;7(3): 487–500.